On the Stability of Pt-Based Catalysts in HBr/Br2 Solution

DOI: 10.1002/hlca.202100082

FULL PAPER

HELVETICA chimica acta

On the Stability of Pt-Based Catalysts in HBr/Br_2 Solution

Qiang Liu,[a] Hubert Meissel,[b] Ilia Sadykov,[c] Simon Jones,[b] Nick Van Dijk,[b] Przemyslaw Rzepka,[a, d] Luca Artiglia,[d, e] Marco Ranocchiari,[d] and Jeroen A. van Bokhoven*[a, d]

[a] Department of Chemistry and Applied Biosciences, Institute for Chemical and Bioengineering, ETH Zurich, Vladimir Prelog Weg 1, CH-8093 Zurich, Switzerland, e-mail: jeroen.vanbokhoven@chem.ethz.ch

[b] TFP Hydrogen Products Ltd., Unit 5 & 6, Merchants Quay, Pennygillam Industrial Estate, UK-Launceston, PL15 7QA, United Kingdom

[c] Operando spectroscopy group, Paul Scherrer Institute, CH-5232 Villigen PSI, Switzerland

[d] Laboratory for Catalysis and Sustainable Chemistry, Paul Scherrer Institute, CH-5232 Villigen PSI, Switzerland

[e] Laboratory of Environmental Chemistry, Paul Scherrer Institute, CH-5232 Villigen PSI, Switzerland

Dedicated to Prof. *Antonio Togni* on the occasion of his 65th birthday.

Stability studies on supported metal nanoparticles are essential for gaining insight into the design and optimization of high-performance materials. In this work, the dissolutions of Pt-based catalysts in HBr/Br_2 mixture of various concentration regimes were studied and correlated with material structural properties. The dissolution of metal nanoparticles was enhanced by adding Br_2 to the HBr solution. Comparing with commercial Pt/C catalyst, the well-alloyed PtIr/C catalyst was observed to exhibit high resistance towards dissolution. In addition, regulating the accessibility of the metal sites to dissolution-inducing species contributed to the marked stability of the nanoparticles in HBr/Br_2 solutions, as shown for the surface-modified PtIr/C catalysts with organic diamine molecules.

Keywords: bromine, hydrobromic acid, metal dissolution, stability, supported catalysts.

Introduction

Heterogeneous catalysts, consisting of metal nanoparticles (NPs) and a solid support, are widely applied in energy-related fields.[1–3] Precious metal-based catalysts such as Pt/C (platinum NPs supported carbon material) hold great promise for a number of catalytic transformations. Challenges associated with unstable performance and easy deactivation limit the practical application of these catalysts.[4–6] Deactivation tends to become more severe for supported metal-based catalysts at high temperatures as well as in an oxidizing atmosphere and in condensed corrosive solvents. An in-depth understanding of catalyst deactivation is, therefore, crucial for the rational design and optimization of (electro)catalysts with high stability.[7–9]

During cell operations, the direct contact with liquid electrolytes and continuous potential fluctuations usually put a greater demand on the durability of electrocatalysts, because electrocatalytic properties can be critically hindered by catalyst degradation.[10–16] The degradation of supported metal NPs is generally reported to originate from dissolution, detachment from the support, coalescence and sintering.[17–20] In particular, metal NPs dissolution usually occurs through direct chemical reactions with reactants and/or electrolyte components accompanied by (electro)catalytic oxidation and reduction processes.[9,11,13,21,22] As well as being determined by the intrinsic structural properties of the catalyst, the intensity of the dissolution of supported metal NPs tends to vary, depending on the applied operating conditions in energy conversion and storage

Supporting information for this article is available on the WWW under https://doi.org/10.1002/hlca.202100082

devices.[23–25] For instance, hydrogen-bromine redox flow batteries (H_2-Br_2 RFBs) involve highly reversible reactions at the anode and cathode side by flowing with H_2 gas and acid electrolyte composed of protons (H^+) and oxidizing Br_x species. Platinum-based catalysts still serve as the most active H_2-related electrode materials. Considerable degradation in performance often occurs due to the strong and irreversible sorption/oxidation property of Br_x on Pt metal surface.[26–28] Long-term practical durability of Pt-based catalysts is hence desirable when contacting with highly concentrated HBr/Br_2 solutions in H_2-Br_2 RFBs. In this regard, the studies on how the carbon-supported Pt-based NPs dissolve in Br_x-containing solutions and the factors that influence this can aid in optimizing and improving catalyst dissolution resistance. Up to now, however, only a few such stability studies have been published; their focus is mainly on the dipping of the Pt-based catalyst into an acidic HBr solution without Br_2 before carrying out electrical measurements.[29,30]

Here, we report on the systematic evaluation of the stability of Pt/C with a regulated particle size and PtIr/C consisting of PtIr alloy NPs in HBr/Br_2 solution with different concentration regimes. Polybromide anions (*i.e.*, Br_3^-) in the HBr/Br_2 solution accelerated the dissolution of metal NPs. Metal dissolution rates depend to a great extent on the size of the NPs and the surface property rather than on the concentration of Br_2 in the investigated HBr/Br_2 solutions. Sterically limited accessible sites on the PtIr/C-based catalysts after surface organic modification were responsible for the observed marked resistance towards dissolution. The findings in this work serve to provide proper guides on the design of durable (electro)catalysts, which are applied especially in HBr/Br_2 solution-involved catalytic system, such as membraneless H_2-Br_2 RFBs.

Results and Discussion

Structural and Dissolution Properties of the Pt/C Catalysts

The studies on the dissolution of carbon-supported metal NPs began with the selection of the commercial Pt/C catalyst (*Alfa Aesar*), the catalyst which is used most frequently in electrocatalytic transformations. Inductively coupled plasma optical emission spectrometry (ICP-OES) analysis demonstrated that 40 wt-% of Pt was loaded on carbon. *Figure 1,a* is the TEM image of Pt NPs with a diameter of 1.0–2.0 nm, uniformly dispersed on the support. In order to investigate the effect of particle size on metal dissolution, Pt/C was annealed at 350 °C and 700 °C in a N_2 atmosphere. Carbon-supported Pt NPs with a mean diameter of 3.5 nm and 5.0 nm were obtained on the Pt/C-350 and Pt/C-700, respectively (*Figure 1,b* and *1,c*). When Pt/C is not heated, it is referred to as Pt/C-uncal.

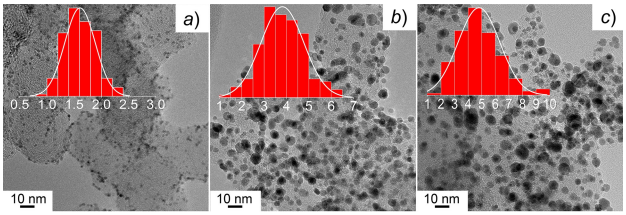

Figure 1. Transmission electron microscopy (TEM) images of *a*) Pt/C-uncal., *b*) Pt/C-350 and *c*) Pt/C-700 catalyst. The insets are the corresponding particle size distribution histograms. All scale bars are 10 nm.

Table S1 (*Supporting Information*) lists the concentrations of the solutions in the HBr/Br_2 series. In practical H_2-Br_2 RFBs, the concentration of Br species in the electrolyte at different states of charge is around 6–8 M (M: molar L^{-1}) to meet the requirement on power density. In this regard, HBr/Br_2 solutions in our work with the concentration of 5.6 M/0.6 M, 4.8 M/0.9 M, 4.0 M/1.3 M, 3.2 M/1.7 M, 2.4 M/2.1 M represent the electrolyte compositions due to the Br^-/Br_2 redox reactions in H_2-Br_2 RFBs. All the dissolution experiments in this work were carried out at room temperature (25.0 °C). *Figure 2,a* presents Pt NPs dissolution profiles for the Pt/C catalysts after 16 h in HBr solution with a concentration ranging from 8.2 M to 2.4 M. The highest degree of dissolution (66%) was found for the Pt/C-uncal. in 8.2 M HBr, while that were much lower for Pt/C-350 and Pt/C-700 having larger metal particle size. With a decrease in HBr concentration, the degree of Pt dissolution also tends to decrease. In comparison, however, as shown in *Figure 2,b*, severe dissolution (more than 80%) of Pt NPs from Pt/C-uncal. and Pt/C-700 had taken place in HBr/Br_2 solutions after 2 h. Even when the reaction time was reduced to 40 min, the extent of Pt dissolution was still high (over 60%). All the investigated Pt/C-uncal., Pt/C-350 and Pt/C-700 exhibited almost complete Pt dissolution in HBr/Br_2 solutions when immersing for 16 h (*Figure S1*). The above results indicate that nanoparticle size played an important role in the dissolution of Pt NPs in acidic HBr solution, because the surface amount of low-coordinated atoms and the chemical potential for dissolution vary with the size of nanoparticles.[11,31] Besides, the addition of Br_2 into the HBr solution can

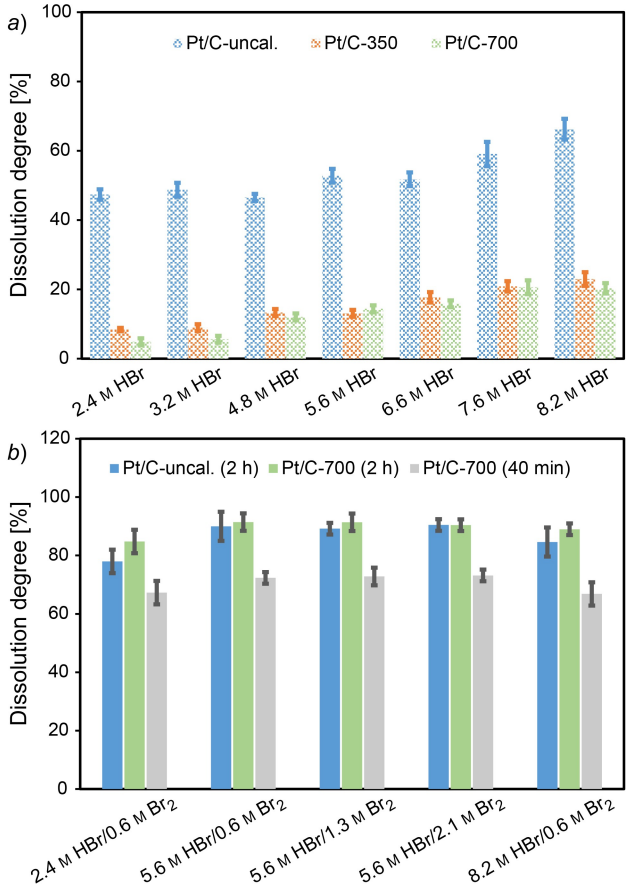

Figure 2. Degree of dissolution of Pt NPs from Pt/C catalysts in *a*) HBr after 16 h and *b*) HBr/Br_2 mixture after 2 h and 40 min. The colors indicate the catalysts and reaction time in the columns with error bars.

significantly accelerate the dissolution of Pt NPs. As shown in *Figure S2*, the enhancement of Pt dissolution by adding Br_2 to the HBr solution was more remarkable for 2.4 M HBr with the highest Br_2 concentration (2.1 M).

In bromide/bromine-containing solution, polybromide complexes such as tribromide (Br_3^-) and pentabromide (Br_5^-) anions are formed through the *Eqns. 1* and *2*:

$$Br^- + Br_2 \rightleftharpoons Br_3^- \quad (1)$$

$$Br^- + 2\,Br_2 \rightleftharpoons Br_5^- \quad (2)$$

The equilibrium constant for the formation of Br_3^- and Br_5^- anions are expressed by *Eqns. 3* and *4*. Earlier literatures have reported the K_3 value in the range of 16 to 20 $L\,mol^{-1}$ (at 25.0 °C),[32–35] while that of K_5 is between 19 and 41 $L^2\,mol^{-2}$.[33–36]

$$K_3 = \frac{[Br_3^-]}{[Br_2]^*[Br^-]} \quad (3)$$

$$K_5 = \frac{[Br_5^-]}{[Br_2]^{2*}[Br^-]} \quad (4)$$

The $[Br_5^-]$, $[Br_3^-]$, $[Br_2]$ and $[Br^-]$ refer to the equilibrium concentration of Br_5^-, Br_3^-, Br_2 and Br^- in the HBr/Br_2 solution, respectively.

For the series of HBr/Br_2 solution employed for the dissolution of Pt/C, the equilibrium concentration of Br^-, Br_2 and polybromide (Br_3^- and Br_5^-) anions were simulated based on the initial concentration of HBr and Br_2, as well as the K_3 (16 $L\,mol^{-1}$) and K_5 (37 $L^2\,mol^{-2}$).[37] As shown in *Figure S3*, Br_2 was almost dissolved in the highly concentrated HBr solution by forming Br_3^- as the dominant species (more than 95 %). Then we performed ultraviolet visible spectrometry (UV-Vis) measurements on the solution before and after Pt/C dissolution. Typically, from the spectra of 5.6 M HBr/0.6 M Br_2 (*Figure S4,a*), the adsorption peak at 267 nm was likely assigned to the Br_3^- species,[38,39] and the contributions by other polybromide anions such as Br_5^- and Br_7^- could not be ruled out. While that observed at 390 nm, with a much lower intensity, was the adsorption of Br_2.[40] The UV-Vis analysis indicated that it is the polybromide anions formed through Br^-/Br_2 equilibrium reactions rather than the bromide (Br^-) that play a crucial role in enhancing the dissolution of carbon-supported Pt NPs. Furthermore, the bromoplatinic acid complex was distinguished from the two broad peaks centered at 315 and 260 nm in the UV-Vis spectra.[41,42] This metal complex was also observable in pure HBr solution (comprising protons and Br^- anions) after the dissolution of Pt/C, which suggests that both Br^- and polybromide anions participated in the formation of Pt complexes in the HBr/Br_2 solution.

Structural and Dissolution Properties of the PtIr/C Catalysts

After studying the dissolution of Pt/C, PtIr alloys became the focus of the investigation on metal nanoparticle dissolution in HBr/Br_2 solutions. It has already been shown that PtIr alloyed catalysts are active in various electrocatalytic reactions.[43–46] We obtained a PtIr/C catalyst with 40 wt-% metal loading on carbon material from *TFP Hydrogen Products Ltd.*. This catalyst was developed to exhibit much higher activity than the commercial Pt/C towards the hydrogen evolution reaction (HER), which is the half-cell

reaction on the anode side of H_2-Br_2 RFBs. Carbon-supported PtIr NPs were characterized to be polycrystalline nature with a particle size distribution between 30 and 40 nm from the TEM images (*Figure 3,a* and *3,b*). PtIr NPs were additionally observed to have porous nano-dendritic structures. It is worth noting that the particle size (6.6 ± 0.2 nm) of PtIr calculated based on XRD measuring is in essence not in agreement with that from TEM. It points out the PtIr nano-dendritics are formed by the aggregations of small nanoparticles during the synthesis. The bulk composition of PtIr NPs was found to have a Pt/Ir atomic ratio of 80 : 20, based on the analysis of energy-dispersive X-ray (EDX) spectra (*Figure S4,c*). HAADF-STEM mapping images (*Figure 3,c*) suggested that Pt and Ir were well-dispersed on the PtIr NPs, but they did not display the characteristic core-shell structure. The collected XRD pattern shown in *Figure 3,d* revealed the reflections at 39.93°, 46.42°, 67.83°, 81.57° 2θ angles, which were indexed as (111), (200), (220) and (311) planes of typical face-centered cubic (fcc) structure of Pt.[47] The absence of any phase of Ir (Ir^0 JCDPS# 87-0715; IrO_x JCDPS# 88-0288) stands in line with the formation of a PtIr alloy phase in the resulting PtIr/C catalyst.[44,46] The lattice constant for PtIr/C was refined in the space group $Fm\bar{3}m$ to be 3.9076 Å and PtIr NPs had a nearly 100% of alloying degree,[45] as compared with that (3.9038 Å) calculated from *Vegard*'s law. These findings proved the formation of well-alloyed PtIr NPs on the prepared PtIr/C catalyst.

The extent of PtIr/C dissolution was evaluated under the similar conditions as for Pt/C. There was a gradual decrease in the amount of dissolved Pt from PtIr/C in the concentrated HBr as well as in the HBr/Br_2 solutions. In contrast to Pt/C, the enhancement of Pt dissolution as a result of adding Br_2 to the HBr was not as strong in the case of 2.4 M HBr/2.1 M Br_2, compared to that of 8.2 M HBr/0.3 M Br_2 (*Figure 4*). A similar tendency was found for Ir on PtIr/C (*Figure S5*). The lower degree of metal dissolution compared with Pt/C was probably a consequence of the distinct surface structure and the self-stability of PtIr nano-dendritics on PtIr/C. Furthermore, negligible metal dissolution occurred on PtIr/C when HBr was replaced by KBr in the case of 4.0 M KBr/1.3 M Br_2 (*Figure S6*). This confirmed that the synergy between highly concentrated H^+ and the as-formed polybromide anions was linked to the rapid dissolution of carbon-supported Pt-based NPs.

The respective dependence of HBr and Br_2 on concentration with regard to the dissolution of PtIr NPs in a variety of HBr/Br_2 media was checked. *Table S1* also shows the concentrations of HBr/Br_2 solution employed in this concentration-dependent study. The simulated concentrations of polybromide equilibria and Br_2 in these HBr/Br_2 solutions are plotted into *Figure 5,a* and *Figure 5,c*. Increasing the concentration of the initially added Br_2 could induce the formation of Br_5^- anions, but still maintain Br_3^- as the dominant species. The formation of heptabromide

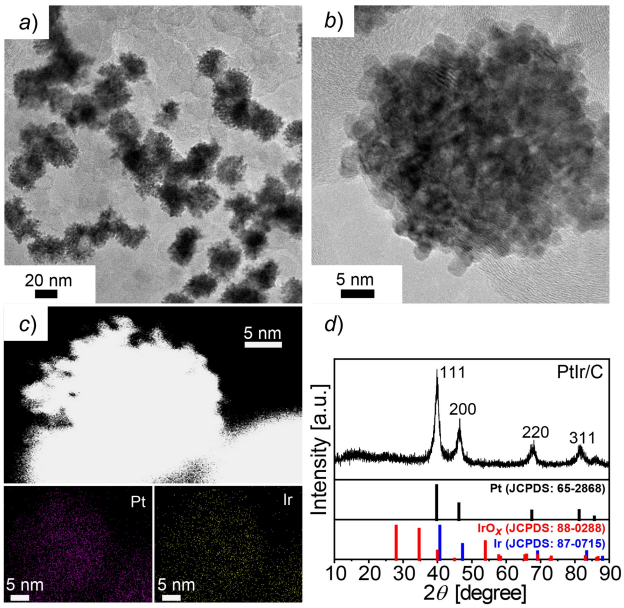

Figure 3. TEM (*a*), high resolution TEM (*b*) and high-angle annular dark field scanning transmission electron microscopy (HAADF-STEM) mapping (*c*) images of PtIr/C. Scale bars are set as presented on the corresponding images. *d*) X-ray powder diffraction (XRD) pattern of PtIr/C with the standard X-ray diffraction lines of metallic Pt, Ir, and IrO_x plotted below.

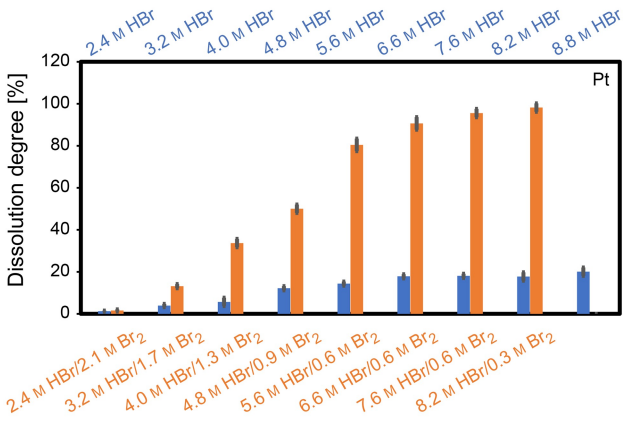

Figure 4. Comparison of degree of dissolution of Pt from PtIr/C catalyst after the period of 16 h in the HBr (blue) and HBr/Br_2 mixtures (light brown).

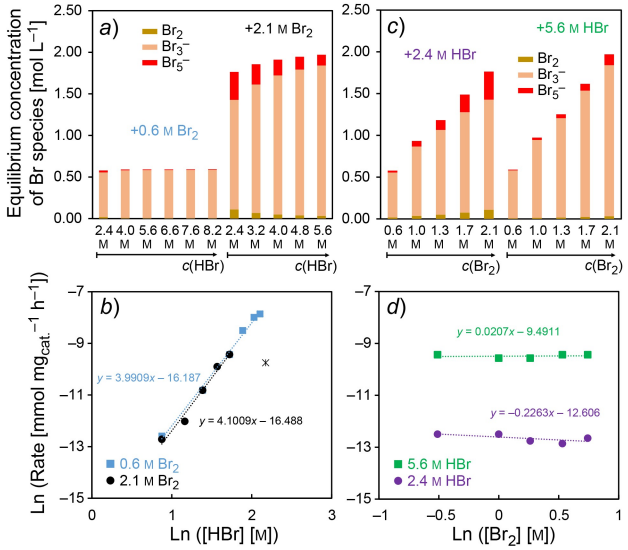

Figure 5. Simulated concentration of Br^-, Br_2, Br_3^- and Br_5^- in HBr/Br_2 solutions for the dependence study on *a*) HBr and *c*) Br_2 concentration. Pt dissolution rates as function of the concentration of HBr (*b*) by keeping the concentration of Br_2 as a constant (0.6 and 2.1 M); while that on the concentration of Br_2 (*d*), 5.6 and 2.4 M of HBr were applied to prepare the HBr/Br_2 solution series.

(Br_7^-) species at higher Br_2 concentrations should not be ruled out.[37] Their exact amount, however, cannot be determined due to the lack of the equilibrium constant of Br_7^- from the literature. *Figure 5,b* shows the rate of Pt dissolution (Ln(mmol/$mg_{cat.}$/h); Ln is the natural logarithm function. There is a positive trend as a function of Ln([HBr]), showing a reaction order of *ca.* 4. However, a near-zero reaction order was determined from the dependence on Br_2 concentration (*Figure 5,d*). The dissolution of Ir from the PtIr/C also exhibited similar concentration-dependent properties (*Figure S7*). These findings demonstrated that polybromide anions in HBr/Br_2 solution could easily get adsorbed on the surface of metal without transport/diffusion limitation.[48] The dissolution of metal was supposed to be started through the dissociative reaction of adsorbed polybromide anions through the Br–Br bond cleavage on the metal sites and then eventually form the metal-bromide complexes. The representative UV-Vis spectra of the HBr/Br_2 solution after PtIr/C dissolution showed a decreased intensity of the adsorption peak of polybromide species (*Figure S8,a*), which was most likely due to changes of the equilibrious state of HBr/Br_2 solution after the formation of bromoplatinic acid and Ir-bromide complexes.

The representative XRD patterns in *Figure S8,b* with decreasing intensities of the diffraction peaks corresponding to the (111), (200) and (220) planes of the alloy structure verified the different degrees of dissolution of PtIr NPs following ICP-OES analysis. The TEM images of PtIr/C (*Figure S9*) illustrated that the evolution of the morphological structure of PtIr NPs or their absence from the carbon support are indicative of severe dissolution. TEM images did not show detectable re-deposition of metal cations onto the carbon support by forming smaller clusters or nanoparticles. This re-deposition can be ruled out, because the PtIr/C catalyst was exposed to highly oxidizing conditions, the formed metal-bromide complexes are usually stable in HBr/Br_2 solution and, more importantly, thorough rinsing with deionized water was performed during the catalyst separation process. It is noteworthy that PtIr NPs exhibited a hollow-like nanostructure after dissolution in the HBr/Br_2 solution (*Figure S9*), whereas it retained its spherical solid structure on the catalyst after dissolution in HBr without Br_2. One explanation may be that polybromide anions, such as Br_3^-, when adsorbed on the surface of metal, form a driving force for the outward diffusion of the inner metal atoms during the dissolution of PtIr NPs, identical to the *Kirkendall* effect in the synthesis of hollow-structured nanocatalysts.[49]

X-ray photoelectron spectroscopy (XPS) measurements were carried out to detect the surface composition and oxidation state of PtIr/C before and after dissolution. In the high-resolution Pt 4f spectra of fresh PtIr/C (*Figure 6,a*), the doublet peaks with a binding energy (BE) of 71.8 and 75.1 eV represented metallic Pt, while the second doublet pairs at 73.0 and 76.3 eV were assigned to oxidized Pt^{2+}.[45] In addition, from the Ir 4f XPS spectra, peaks ascribed to metallic Ir (61.3 and 64.3 eV) and oxidized Ir (62.4 and 65.4 eV) were observed.[50] Surface analysis indicated that Ir was relatively more abundant on the surface of PtIr NPs than in the alloyed phase of the inner bulk; the Pt/Ir atomic ratio was 59:41. Metallic Pt^0 (77%) and Ir^0 (64%) were dominant on PtIr/C together with the appearance of surface cationic metal species (higher BEs), which was confirmed by X-ray absorption spectroscopy (*vide infra*). Surface adsorbed Br^- and covalently coordinated Br species were also detected on the surface of dissolved materials.[51,52] The deconvolution analysis of core-level spectra indicated that both Pt and Ir atoms with a metallic and oxidized state tended to dissolve in HBr/Br_2 mixtures. There was no shift in BEs for Pt, while the Ir doublet peaks showed a positive shift after different levels of dissolution. Moreover, the surface atomic ratio of Pt/Ir decreased as dissolution processed (*Table S2*), suggesting that sur-

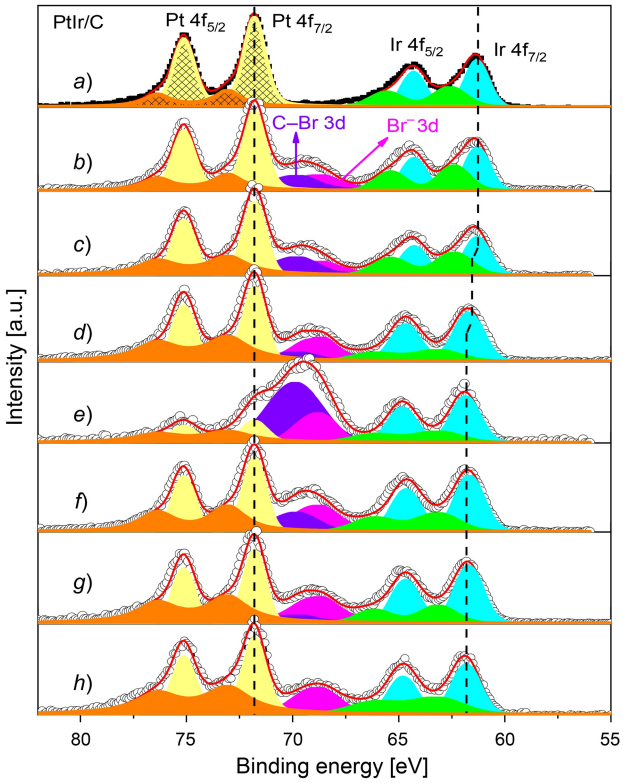

Figure 6. High-resolution Pt 4f, Br 3d and Ir 4f spectra of PtIr/C materials dissolved under different HBr/Br_2 conditions compared to fresh PtIr/C (*a*). The conditions of dissolution are: *b*) 4.0 M HBr/2.1 M Br_2 3 h; *c*) 4.0 M HBr/0.6 M Br_2 3 h; *d*) 5.6 M HBr/0.6 M Br_2 3 h; *e*) 5.6 M HBr/0.6 M Br_2 48 h; *f*) 4.0 M HBr/0.6 M Br_2 48 h; *g*) 4.0 M HBr/2.1 M Br_2 48 h; h) 8.8 M HBr 48 h.

face-exposed Pt on PtIr NPs dissolved more easily than Ir. The observed positive shift of BEs for Ir and the high dissolution extent of Ir from PtIr/C was probably due to the disruptive effect of Pt dissolution, which might increase the amount of less stable low-coordinated surface Ir atoms.[53]

Structural and Dissolution Properties of the Surface Organic-Patterned PtIr/C

Molecular patterning of the surface of metal by organics with $-NH_2$ functional groups is one of the effective strategies for enhancing the electrocatalytic properties of Pt-based electrocatalysts.[54–57] The fundamental basis of this strategy relies on the surface-engineered modifications by regulating the accessibility of metal sites to corrosive and/or poisoning adsorbates such as PO_4^{3-}, SO_4^{2-} and crossover-obtained methanol molecule, *etc.* Inspired by this strategy, we fabricated several organic molecules (*Figure 7*), including cyclohexylamine (L1), aniline (L2), ethylenediamine (L3) and benzene-1,4-diamine (L4), onto the surface of PtIr NPs by using a facile dipping approach, followed by rinsing and drying steps (detailed in the *Supporting Information*). 5.6 M HBr/0.6 M Br_2 was selected for the evaluation of the stability of surface organic-modified catalysts, because it can induce a high degree of dissolution of PtIr/C after a certain time (*Figure 4*). From the dissolution in 5.6 M HBr/0.6 M Br_2 for 16 h, all the surface organic modified catalysts, with the exception of PtIr/C-L1, showed a marked decrease in the amount of dissolved Pt. In particular, as shown in *Figure 7*, 7.8% and below 1.0% of Pt dissolved from PtIr/C-L3 and PtIr/C-L4, respectively, which was significantly lower than the un-modified PtIr/C (80%). As expected, the dissolution of Ir species in PtIr/C-L3 and PtIr/C-L4 was undetectable under the given conditions.

A negligible amount of Pt and Ir dissolved from the PtIr/C catalyst during the surface organic modification, as indicated by the ICP-OES analysis of the L4 diamine-containing ethanol solution. Elemental mapping images of PtIr/C-L4 (*Figure 8,a* and *Figure S10*) illustrated that PtIr NPs had retained their geometric properties in terms of particle size, morphology or shape following surface organic modification. Due to the strong interactions between metal atoms and $-NH_2$ groups,[58,59] organic diamine molecules were still

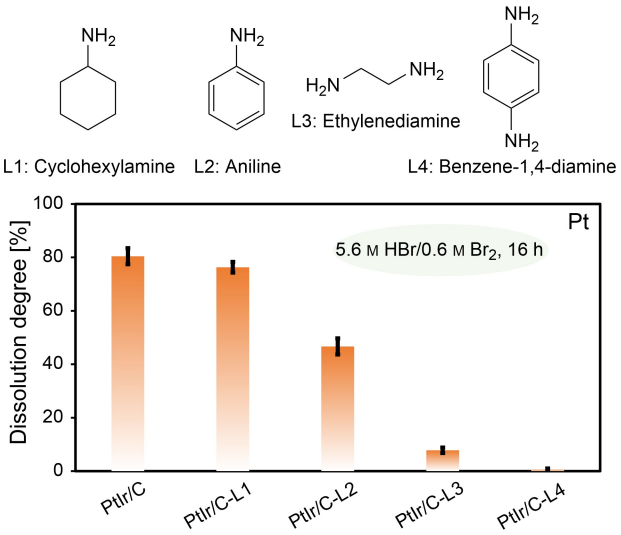

Figure 7. Dissolution of Pt from the un-modified PtIr/C and surface organic-modified PtIr/C after immersing in 5.6 M HBr/0.6 M Br_2 for 16 h. The molecular structures of the amines and diamines selected for the surface organic modifications of PtIr/C are presented above the dissolution column chart.

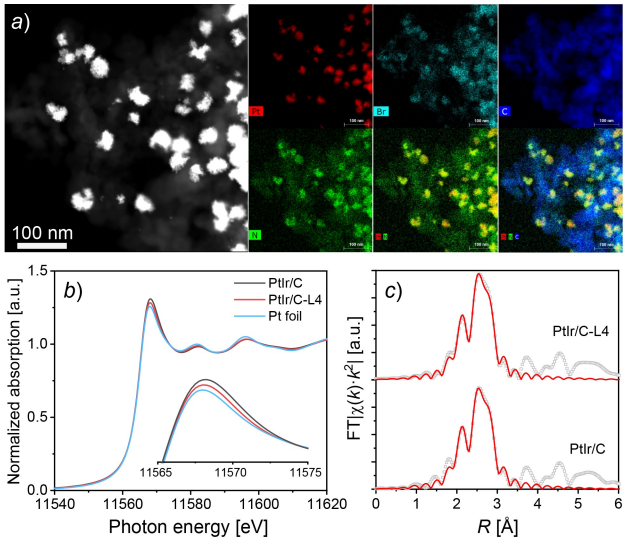

Figure 8. *a*) HAADF-STEM and EDX mapping images of PtIr/C-L4 after dissolution in 5.6 M/0.6 M HBr/Br_2 for 16 h. The normalized XANES spectra at the Pt L_3-edge *b*) of PtIr/C, benzene-1,4-diamine-modified PtIr/C (PtIr/C-L4) compared with corresponding Pt foil spectra. The inset is the comparison of the white-line intensity of measured samples. *c*) Pt L_3-edge EXAFS fitting results of PtIr/C and PtIr/C-L4. The original EXAFS spectra were represented by grey open circles, while the red line represents the corresponding fitting. The spectra exhibit the *Fourier* transformation of the intensity of k^2 weight as a function of *R* (the distance between the center atom and scattering atoms).

observed on the catalyst surface after the dissolution experiments (*Figure S11*).

The improvement in stability was studied by X-ray absorption spectroscopy (XAS) characterization of PtIr/C and PtIr/C-L4. As displayed in *Figure 8,b*, the white line of the Pt L_3-edge decreased, possibly due to surface reduction of PtIr NPs by diamine molecules possessing electron-donating $-NH_2$ groups. It was estimated from Pt L_3-edge extended X-ray absorption fine structure (EXAFS) analysis (*Figure 8,c*, *Table S3*) that the first shell coordination number of both samples is about 10, which is characteristic of Pt nanoparticles.[60] Since there is almost no difference between Pt and Ir absorbers, which have similar backscattering amplitudes and lattice parameters, it is impossible to distinguish between Pt or Ir atoms. Linear combination fitting of the Pt L_3-edge X-ray absorption near edge structure (XANES) for PtIr/C (*Figure S12*) suggested that Pt may be present in an oxidized form, which accounts for only less than 5.5% of the total amount of Pt. Oxidized Pt species are, thus, ascribed to those species that are distributed on the surface of PtIr NPs, as shown by XPS (*Figure 6*). The lower amount (2.8%) of oxidized Pt after surface organic modification confirmed the formation of interactions between metal atoms and diamine molecules (L4) on PtIr NPs.

An evaluation of the accessible number of metal sites on PtIr NPs after surface organic modification by amine or diamine molecules was carried out. Pulse CO-chemisorption measurement (at 35 °C) was performed, a commonly employed technology to determine the dispersion of metal NPs on metal-based catalysts. Metal dispersion was found to decrease due to surface occupation by the organic molecules through interactions between metal atoms and $-NH_2$ groups of amine molecules.[58,59] In particular, among the surface organic-modified samples, at least 85% of the surface sites on PtIr/C-L4 was lost (*Figure S13*). It is noteworthy that the synergy between highly concentrated H^+ and polybromide anions accelerates the dissolution of metal NPs in acidic and oxidizing HBr/Br_2 solutions. The marked stability of PtIr/C-L4 can, therefore, be explained by the steric limitation of accessibility of the metal surface to these dissolution enhancers, in particular, the polybromide anions.

The surface patterned molecules are beneficial for regulating the adsorption of spectator species on metal particle at the expense of blocking certain number of active sites, which is well documented in the literature in electrocatalysis field.[54,55,57] Regarding this, we further collected the cyclic voltammograms of PtIr/C and surface organic-modified PtIr/C at a scan rate of 20 $mV\,s^{-1}$ in 0.5 M H_2SO_4 solution under Ar. The electrochemical surface area (ECSA), a critical parameter for electrocatalytic property, was calculated based on the hydrogen desorption charge as 0.21 μC mg_{Pt}^{-2}.[55] The modification with L1, L2 and L4 organic was observed to decrease 22–25% of ECSA, while that of L3-modified PtIr/C showed 13% of loss (*Figure S14*). These results indicate that the surface organic-modified PtIr/C catalysts might possess the potential activities for the H_2-related oxidation/evolution reactions, in particular, in the H_2-Br_2 RFBs. Evaluations on the performance of these catalysts in terms of electrocatalytic activity and stability are undergoing and will be covered in the following report.

Conclusions

In summary, the results of the present study show that the synergy between acidic H^+ and polybromide anions (*i.e.*, Br_3^- and Br_5^-) in HBr/Br_2 solution contributed to the high level of dissolution of Pt-based nanoparticles from the carbon support. PtIr/C material,

which was characterized to feature well-alloyed and nanodendritic structural property, was more stable than Pt/C under similar dissolution conditions. Surface organic modification on PtIr nanoparticles by means of diamine molecules was effective in improving the dissolution resistance in acidic and oxidizing HBr/Br_2 solutions. Further studies on the electrocatalytic properties of the surface organic-modified PtIr/C catalysts are necessary to gain an in-depth understanding of the (electro)catalyst degradation mechanism and improvement of electrocatalytic efficiencies.

Notes

The content of this report does not reflect the official opinion of the European Union. Responsibility for the information in this publication lies entirely with the authors.

Acknowledgements

This work has received funding from the European Union's Horizon 2020 research and innovation program under grant agreement No 875524 (project website: https://melodyproject.eu/). We thank Dr. *Frank Krumeich* (The Scientific Center for Optical and Electron Microcopy (ScopeM), ETH Zurich), *Arik Beck* and Dr. *Julian T. C. Wennmacher* for assistance with collecting the electron microscopy images, Dr. *Olga V. Safonova* (SuperXAS beamline, Swiss Light Source synchrotron, Switzerland) for the support on XAS measurement, *Marcia Schoenberg* for proofreading and valuable comments, as well as Dr. *Peter Klusener* (*Shell*, the Netherlands), Dr. *Kamuran Yasadi* (*Elestor*, the Netherlands) and Prof. *Xiaohong Li* (University of Exeter, United Kingdom) for fruitful and extensive discussions.

Author Contribution Statement

J. A. van Bokhoven conceived the research; *Q. Liu* performed the dissolution experiments, analyzed the data, and wrote the manuscript; *H. Meissel*, *S. Jones*, and *N. Van Dijk* contributed the development of PtIr/C catalyst and providing of Pt/C catalyst; *H. Meissel* measured the CV curves of PtIr/C catalyst; *I. Sadykov* measured the XAS and processed the data fitting; *P. Rzepka* assisted with the XRD analysis and refined the XRD data; *L. Artiglia* developed XPS method and helped in analyzing the XPS data; *Q. Liu*, *M. Ranocchiari* and *J. A. van Bokhoven* revised the manuscript. All the authors have approved the final version of this manuscript.

References

[1] M. J. Climent, A. Corma, S. Iborra, 'Heterogeneous Catalysts for the One-Pot Synthesis of Chemicals and Fine Chemicals', *Chem. Rev.* **2011**, *111*, 1072–1133.
[2] P. Munnik, P. E. de Jongh, K. P. de Jong, 'Recent Developments in the Synthesis of Supported Catalysts', *Chem. Rev.* **2015**, *115*, 6687–6718.
[3] M. Shao, Q. Chang, J.-P. Dodelet, R. Chenitz, 'Recent Advances in Electrocatalysts for Oxygen Reduction Reaction', *Chem. Rev.* **2016**, *116*, 3594–3657.
[4] H. L. Xin, J. A. Mundy, Z. Liu, R. Cabezas, R. Hovden, L. F. Kourkoutis, J. Zhang, N. P. Subramanian, R. Makharia, F. T. Wagner, D. A. Muller, 'Atomic-Resolution Spectroscopic Imaging of Ensembles of Nanocatalyst Particles Across the Life of a Fuel Cell', *Nano Lett.* **2012**, *12*, 490–497.
[5] G. Prieto, J. Zečević, H. Friedrich, K. P. de Jong, P. E. de Jongh, 'Towards stable catalysts by controlling collective properties of supported metal nanoparticles', *Nat. Mater.* **2013**, *12*, 34–39.
[6] L. Wang, L. Wang, X. Meng, F.-S. Xiao, 'New Strategies for the Preparation of Sinter-Resistant Metal-Nanoparticle-Based Catalysts', *Adv. Mater.* **2019**, *31*, 1901905.
[7] E. D. Goodman, J. A. Schwalbe, M. Cargnello, 'Mechanistic Understanding and the Rational Design of Sinter-Resistant Heterogeneous Catalysts', *ACS Catal.* **2017**, *7*, 7156–7173.
[8] P. J. Ferreira, G. J. la O', Y. Shao-Horn, D. Morgan, R. Makharia, S. Kocha, H. A. Gasteiger, 'Instability of Pt/C Electrocatalysts in Proton Exchange Membrane Fuel Cells: A Mechanistic Investigation', *J. Electrochem. Soc.* **2005**, *152*, A2256–A2271.
[9] D. J. Myers, X. Wang, M. C. Smith, K. L. More, 'Potentiostatic and Potential Cycling Dissolution of Polycrystalline Platinum and Platinum Nano-Particle Fuel Cell Catalysts', *J. Electrochem. Soc.* **2018**, *165*, F3178–F3190.
[10] C. Spöri, J. T. H. Kwan, A. Bonakdarpour, D. P. Wilkinson, P. Strasser, 'The Stability Challenges of Oxygen Evolving Catalysts: Towards a Common Fundamental Understanding and Mitigation of Catalyst Degradation', *Angew. Chem. Int. Ed.* **2017**, *56*, 5994–6021.
[11] L. Tang, B. Han, K. Persson, C. Friesen, T. He, K. Sieradzki, G. Ceder, 'Electrochemical Stability of Nanometer-Scale Pt Particles in Acidic Environments', *J. Am. Chem. Soc.* **2010**, *132*, 596–600.
[12] S. Chen, H. A. Gasteiger, K. Hayakawa, T. Tada, Y. Shao-Horn, 'Platinum-Alloy Cathode Catalyst Degradation in Proton Exchange Membrane Fuel Cells: Nanometer-Scale Compositional and Morphological Changes', *J. Electrochem. Soc.* **2010**, *157*, A82–A97.
[13] A. A. Topalov, I. Katsounaros, M. Auinger, S. Cherevko, J. C. Meier, S. O. Klemm, K. J. J. Mayrhofer, 'Dissolution of Platinum: Limits for the Deployment of Electrochemical Energy Conversion?', *Angew. Chem. Int. Ed.* **2012**, *51*, 12613–12615.

[14] P. P. Lopes, D. Strmcnik, D. Tripkovic, J. G. Connell, V. Stamenkovic, N. M. Markovic, 'Relationships between Atomic Level Surface Structure and Stability/Activity of Platinum Surface Atoms in Aqueous Environments', *ACS Catal.* **2016**, *6*, 2536–2544.

[15] E. F. Holby, W. Sheng, Y. Shao-Horn, D. Morgan, 'Pt nanoparticle stability in PEM fuel cells: influence of particle size distribution and crossover hydrogen', *Energy Environ. Sci.* **2009**, *2*, 865–871.

[16] G. Lin, P. Y. Chong, V. Yarlagadda, T. V. Nguyen, R. J. Wycisk, P. N. Pintauro, M. Bates, S. Mukerjee, M. C. Tucker, A. Z. Weber, 'Advanced Hydrogen-Bromide Flow Batteries with Improved Efficiency, Durability and Cost', *J. Electrochem. Soc.* **2015**, *163*, A5049–A5056.

[17] P. P. Lopes, D. Li, H. Lv, C. Wang, D. Tripkovic, Y. Zhu, R. Schimmenti, H. Daimon, Y. Kang, J. Snyder, N. Becknell, K. L. More, D. Strmcnik, N. M. Markovic, M. Mavrikakis, V. R. Stamenkovic, 'Eliminating dissolution of platinum-based electrocatalysts at the atomic scale', *Nat. Mater.* **2020**, *19*, 1207–1214.

[18] S. R. Challa, A. T. Delariva, T. W. Hansen, S. Helveg, J. Sehested, P. L. Hansen, F. Garzon, A. K. Datye, 'Relating Rates of Catalyst Sintering to the Disappearance of Individual Nanoparticles during Ostwald Ripening', *J. Am. Chem. Soc.* **2011**, *133*, 20672–20675.

[19] R. Borup, J. Meyers, B. Pivovar, Y. S. Kim, R. Mukundan, N. Garland, D. Myers, M. Wilson, F. Garzon, D. Wood, P. Zelenay, K. More, K. Stroh, T. Zawodzinski, J. Boncella, J. E. McGrath, M. Inaba, K. Miyatake, M. Hori, K. Ota, Z. Ogumi, S. Miyata, A. Nishikata, Z. Siroma, Y. Uchimoto, K. Yasuda, K.-i. Kimijima, N. Iwashita, 'Scientific Aspects of Polymer Electrolyte Fuel Cell Durability and Degradation', *Chem. Rev.* **2007**, *107*, 3904–3951.

[20] H. A. Baroody, D. B. Stolar, M. H. Eikerling, 'Modeling-based data treatment and analytics of catalyst degradation in polymer electrolyte fuel cells', *Electrochim. Acta* **2018**, *283*, 1006–1016.

[21] R. Sharma, S. M. Andersen, 'Quantification on Degradation Mechanisms of Polymer Electrolyte Membrane Fuel Cell Catalyst Layers during an Accelerated Stress Test', *ACS Catal.* **2018**, *8*, 3424–3434.

[22] A. A. Topalov, S. Cherevko, A. R. Zeradjanin, J. C. Meier, I. Katsounaros, K. J. J. Mayrhofer, 'Towards a comprehensive understanding of platinum dissolution in acidic media', *Chem. Sci.* **2014**, *5*, 631–638.

[23] S. Cherevko, G. P. Keeley, S. Geiger, A. R. Zeradjanin, N. Hodnik, N. Kulyk, K. J. J. Mayrhofer, 'Dissolution of Platinum in the Operational Range of Fuel Cells', *ChemElectroChem* **2015**, *2*, 1471–1478.

[24] M. Prokop, M. Drakselova, K. Bouzek, 'Review of the experimental study and prediction of Pt-based catalyst degradation during PEM fuel cell operation', *Curr. Opin. Electrochem.* **2020**, *20*, 20–27.

[25] K. Ehelebe, J. Knöppel, M. Bierling, B. Mayerhöfer, T. Böhm, N. Kulyk, S. Thiele, K. J. J. Mayrhofer, S. Cherevko, 'Platinum Dissolution in Realistic Fuel Cell Catalyst Layers', *Angew. Chem. Int. Ed.* **2021**, *60*, 8882–8888.

[26] M. Goor-Dar, N. Travitsky, E. Peled, 'Study of hydrogen redox reactions on platinum nanoparticles in concentrated HBr solutions', *J. Power Sources* **2012**, *197*, 111–115.

[27] N. Garcia-Araez, J. J. Lukkien, M. T. M. Koper, J. M. Feliu, 'Competitive adsorption of hydrogen and bromide on Pt(100): Mean-field approximation vs. Monte Carlo simulations', *J. Electroanal. Chem.* **2006**, *588*, 1–14.

[28] M. C. Tucker, K. T. Cho, A. Z. Weber, G. Lin, T. V. Nguyen, 'Optimization of electrode characteristics for the Br_2/H_2 redox flow cell', *J. Appl. Electrochem.* **2015**, *45*, 11–19.

[29] G. Gershinsky, P. Nanikashvili, R. Elazari, D. Zitoun, 'From the Sea to Hydrobromic Acid: Polydopamine Layer as Corrosion Protective Layer on Platinum Electrocatalyst', *ACS Appl. Mater. Interfaces* **2018**, *1*, 4678–4685.

[30] K. Saadi, P. Nanikashvili, Z. Tatus-Portnoy, S. Hardisty, V. Shokhen, M. Zysler, D. Zitoun, 'Crossover-tolerant coated platinum catalysts in hydrogen/bromine redox flow battery', *J. Power Sources* **2019**, *422*, 84–91.

[31] K. Kinoshita, 'Particle Size Effects for Oxygen Reduction on Highly Dispersed Platinum in Acid Electrolytes', *J. Electrochem. Soc.* **1990**, *137*, 845–848.

[32] R. O. Griffith, A. McKeown, A. G. Winn, 'The bromine-bromide-tribromide equilibrium', *Trans. Faraday Soc.* **1932**, *28*, 101–107.

[33] D. B. Scaife, H. J. V. Tyrrell, 'Equilibrium Constants for the Reaction between Bromine and Bromide Ions at 5°, 25°, and 35° in Aqueous Medium of Constant Ionic Strength and Acidity', *J. Chem. Soc.* **1958**, 386–392.

[34] R. W. Ramette, D. A. Palmer, 'Thermodynamics of tri- and pentabromide anions in aqueous solution', *J. Solution Chem.* **1986**, *15*, 387–395.

[35] G. Jones, S. Baeckström, 'Equilibria in Aqueous Solutions of Bromine and Potassium Bromide', *J. Am. Chem. Soc.* **1934**, *56*, 1517–1523.

[36] C. M. Kelley, H. V. Tartar, 'On the System: Bromine-Water', *J. Am. Chem. Soc.* **1956**, *78*, 5752–5756.

[37] M. Küttinger, J. K. Wlodarczyk, D. Daubner, P. Fischer, J. Tübke, 'High energy density electrolytes for H_2/Br_2 redox flow batteries, their polybromide composition and influence on battery cycling limits', *RSC Adv.* **2021**, *11*, 5218–5229.

[38] M. Soulard, F. Bloc, A. Hatterer, 'Diagrams of existence of chloramines and bromamines in aqueous solution', *J. Chem. Soc. Dalton Trans.* **1981**, 2300–2310.

[39] M. Lin, P. Archirel, N. T. Van-Oanh, Y. Muroya, H. Fu, Y. Yan, R. Nagaishi, Y. Kumagai, Y. Katsumura, M. Mostafavi, 'Temperature Dependent Absorption Spectra of Br^-, $Br_2^{\bullet-}$, and Br_3^- in Aqueous Solutions', *J. Phys. Chem. A* **2011**, *115*, 4241–4247.

[40] T. X. Wang, M. D. Kelley, J. N. Cooper, R. C. Beckwith, D. W. Margerum, 'Equilibrium, Kinetic, and UV-Spectral Characteristics of Aqueous Bromine Chloride, Bromine, and Chlorine Species', *Inorg. Chem.* **1994**, *33*, 5872–5878.

[41] P.-H. van Wyk, W. J. Gerber, K. R. Koch, 'A robust method for speciation, separation and photometric characterization of all $[PtCl_{6-n}Br_n]^{2-}$ ($n=0$–6) and $[PtCl_{4-n}Br_n]^{2-}$ ($n=0$–4) complex anions by means of ion-pairing RP-HPLC coupled to ICP-MS/OES, validated by high resolution ^{195}Pt NMR spectroscopy', *Anal. Chim. Acta* **2011**, *704*, 154–161.

[42] M. A. Śmiałek, S. Ptasińska, J. Gow, S. V. Hoffmann, N. J. Mason, 'Radio- and photosensitization of DNA with compounds containing platinum and bromine atoms', *Eur. Phys. J. D* **2015**, *69*, 121.

[43] Y.-W. Lee, E.-T. Hwang, D.-H. Kwak, K.-W. Park, 'Preparation and characterization of PtIr alloy dendritic nanostructures with superior electrochemical activity and stability in oxygen reduction and ethanol oxidation reactions', *Catal. Sci. Technol.* **2016**, *6*, 569–576.

[44] X. Gao, L. Liu, Q. Wang, K. Qi, Z. Jin, W. Zheng, X. Cui, 'One-Pot Synthesis of Nanodendritic PtIr Alloy with High Electrochemical Activity for Ethylene Glycol Oxidation', *NANO* **2017**, *12*, 1750026.

[45] S. J. Hwang, S. J. Yoo, T.-Y. Jeon, K.-S. Lee, T.-H. Lim, Y.-E. Sung, S.-K. Kim, 'Facile synthesis of highly active and stable Pt–Ir/C electrocatalysts for oxygenreduction and liquid fueloxidation reaction', *Chem. Commun.* **2010**, *46*, 8401–8403.

[46] S. Lu, K. Eid, Y. Deng, J. Guo, L. Wang, H. Wang, H. Gu, 'One-pot synthesis of PtIr tripods with a dendritic surface as an efficient catalyst for the oxygen reduction reaction', *J. Mater. Chem. A* **2017**, *5*, 9107–9112.

[47] J. Wang, X.-B. Zhang, Z.-L. Wang, L.-M. Wang, W. Xing, X. Liu, 'One-step and rapid synthesis of "clean" and monodisperse dendritic Pt nanoparticles and their high performance toward methanol oxidation and *p*-nitrophenol reduction', *Nanoscale* **2012**, *4*, 1549–1552.

[48] H. A. Gasteiger, N. M. Marković, P. N. Ross, 'Bromide Adsorption on Pt(111): Adsorption Isotherm and Electrosorption Valency Deduced from $RRD_{Pt(111)}E$ Measurements', *Langmuir* **1996**, *12*, 1414–1418.

[49] H. J. Fan, M. Knez, R. Scholz, D. Hesse, K. Nielsch, M. Zacharias, U. Gösele, 'Influence of Surface Diffusion on the Formation of Hollow Nanostructures Induced by the Kirkendall Effect: The Basic Concept', *Nano Lett.* **2007**, *7*, 993–997.

[50] R. D. Kumar, Z. Wang, C. Li, A. V. N. Kumar, H. Xue, Y. Xu, X. Li, L. Wang, H. Wang, 'Trimetallic PdCuIr with long-spined sea-urchin-like morphology for ambient electroreduction of nitrogen to ammonia', *J. Mater. Chem. A* **2019**, *7*, 3190–3196.

[51] V. K. Abdelkader, M. Domingo-García, M. Melguizo, R. López-Garzón, F. J. López-Garzón, M. Pérez-Mendoza, 'Covalent bromination of multi-walled carbon nanotubes by iodine bromide and cold plasma treatments', *Carbon* **2015**, *93*, 276–285.

[52] M. K. Rabchinskii, S. A. Ryzhkov, D. A. Kirilenko, N. V. Ulin, M. V. Baidakova, V. V. Shnitov, S. I. Pavlov, R. G. Chumakov, D. Y. Stolyarova, N. A. Besedina, A. V. Shvidchenko, D. V. Potorochin, F. Roth, D. A. Smirnov, M. V. Gudkov, M. Brzhezinskaya, O. I. Lebedev, V. P. Melnikov, P. N. Brunkov, 'From graphene oxide towards aminated graphene: facile synthesis, its structure and electronic properties', *Sci. Rep.* **2020**, *10*, 6902.

[53] P. Jovanovič, V. S. Šelih, M. Šala, S. Hočevar, F. Ruiz-Zepeda, N. Hodnik, M. Bele, M. Gaberšček, 'Potentiodynamic dissolution study of PtRu/C electrocatalyst in the presence of methanol', *Electrochim. Acta* **2016**, *211*, 851–859.

[54] Y.-H. Chung, D. Y. Chung, N. Jung, Y.-E. Sung, 'Tailoring the Electronic Structure of Nanoelectrocatalysts Induced by a Surface-Capping Organic Molecule for the Oxygen Reduction Reaction', *J. Phys. Chem. Lett.* **2013**, *4*, 1304–1309.

[55] Y.-H. Chung, S. J. Kim, D. Y. Chung, H. Y. Park, Y.-E. Sung, S. J. Yoo, J. H. Jang, 'Third-body effects of native surfactants on Pt nanoparticle electrocatalysts in proton exchange fuel cells', *Chem. Commun.* **2015**, *51*, 2968–2971.

[56] M. Sharma, N. Jung, S. J. Yoo, 'Toward High-Performance Pt-Based Nanocatalysts for Oxygen Reduction Reaction through Organic–Inorganic Hybrid Concepts', *Chem. Mater.* **2018**, *30*, 2–24.

[57] L. Lu, Z. Wang, S. Zou, Y. Zhou, W. Hong, R. Li, L. Xiao, J. Liu, X.-Q. Gong, J. Fan, 'Ligand-mediated bifunctional catalysis for enhanced oxygen reduction and methanol oxidation tolerance in fuel cells', *J. Mater. Chem. A* **2018**, *6*, 18884–18890.

[58] G.-R. Xu, B. Wang, J.-Y. Zhu, F.-Y. Liu, Y. Chen, J.-H. Zeng, J.-X. Jiang, Z.-H. Liu, Y.-W. Tang, J.-M. Lee, 'Morphological and Interfacial Control of Platinum Nanostructures for Electrocatalytic Oxygen Reduction', *ACS Catal.* **2016**, *6*, 5260–5267.

[59] F.-M. Li, X.-Q. Gao, S.-N. Li, Y. Chen, J.-M. Lee, 'Thermal decomposition synthesis of functionalized PdPt alloy nanodendrites with high selectivity for oxygen reduction reaction', *NPG Asia Mater.* **2015**, *7*, e219.

[60] C.-S. Lin, M. R. Khan, S. D. Lin, 'The preparation of Pt nanoparticles by methanol and citrate', *J. Colloid Interface Sci.* **2006**, *299*, 678–685.

Received May 28, 2021
Accepted May 28, 2021

